# Experimental investigation of neck propagation in polymers

**A. Marquez-Lucero*, C. G'Sell**
*Laboratoire de Physique du Solide (U.A. CNRS 155), Ecole des Mines, Parc de Saurupt, 54042 Nancy Cedex, France*

**and K. W. Neale†**
*Faculté des Sciences Appliquées, Université de Sherbrooke, Sherbrooke, Québec, Canada J1K 2R1*
*(Received 24 June 1988; accepted 23 August 1988)*

Neck propagation is investigated for two different thermoplastic polymers (high density polyethylene and polyethylene terephthalate) at room temperature and at several elongation rates. Two types of tensile test were performed: axisymmetric and plane-strain. The tests were performed under both isothermal and non-isothermal conditions. The results are displayed using a description developed by Neale *et al.* where the specimen neck profiles are simulated by hyperbolic tangent functions.

**(Keywords: polyethylene; polyethylene terephthalate; neck propagation; isothermal; non-isothermal; plastic instability)**

## INTRODUCTION

In many engineering thermoplastics under stretching, a substantial part of the plastic deformation occurs in an unstable way. This is more readily observed in amorphous polymers at a temperature close to or lower than the glass transition temperature, $T_g$, and for semi-crystalline polymers between $T_g$ and the melting temperature, $T_m$. Plastic instability manifests itself in the form of a neck which localizes at some region of the material and then spreads along the length of the specimen. Thus two regions develop: the unnecked region and the necked one. A transition zone divides these two regions, commonly termed the 'shoulder'[1–3], or the 'transition front'[4,5]. The overall load–stretch curve for such a test first shows a maximum, corresponding to the onset of necking, followed by a gradual unloading which corresponds to neck localization and eventual stabilization[6]. With further straining the load essentially remains constant while the neck propagates. Finally, when the neck covers the entire specimen, the load increases until the specimen fails.

Neck propagation in polymers has been extensively studied in the literature[1–15]. However, the experimental data that can be found are normally limited to some particular aspects of the global phenomena.

The objective of the present work is to provide more complete information for neck propagation in two thermoplastic polymers at several stretching rates. To describe the observed behaviour, we have used a characterization procedure based on Reference 4, where the neck profile is represented by a hyperbolic tangent function.

## EXPERIMENTAL PROCEDURE

### *Materials*

Two materials were chosen for the present study: cylindrical rods 20 mm in diameter of a high density polyethylene (HDPE) manufactured by Union Carbide Limited, Canada, and extruded by Plastifab Inc. of Montréal; and a 150 $\mu$m thick film sample of polyethylene terephthalate (PET) extruded by Rhône-Poulenc Film Division of Lyon, France. Optical microscopy and birefringence measurements were carried out on both materials to verify that they did not contain any significant structural or micro-morphological inhomogeneities. In *Table 1* the main structural parameters and industrial references of the materials are reported.

### *Tensile tests*

Principally two types of tensile tests were performed: axisymmetrical and plane-strain. The former were performed using axisymmetric HDPE specimens as shown in *Figure 1a* while the latter were performed using PET film specimens, as shown in *Figure 1b*.

To trigger a controlled neck initiation, a defect was introduced in the central zone of the film specimens. Also, these specimens were marked with three rows of fine dots parallel to the tensile axis (by means of the Letraset dry marking technique) to determine the distribution of strains under stretching.

The axisymmetric tensile tests were performed at $25 \pm 2$°C and at stretching rates ranging from $4 \times 10^{-4}$ to 1 mm s$^{-1}$, while the plane-strain tensile tests were carried out at $21 \pm 1$°C, and at stretching rates ranging between $3 \times 10^{-3}$ and 3 mm s$^{-1}$. A computerized hydraulic Instron machine (Model 8032) was used for all the experiments. The evolution of the specimen profiles during the tests was followed photographically using an Olympus camera mounted to face the sample and

* Present address: National Research Council of Canada, Industrial Materials Research Institute, Boucherville, Québec, Canada J4B 6Y4
† To whom correspondence should be addressed

0032-3861/89/040636-07$03.00

**Table 1** Structural parameters and industrial references for HDPE and PET

| | HDPE | PET |
|---|---|---|
| $\bar{M}_w$ (weight average molecular mass) | 192 200 | 40 000 |
| Density (g cm$^{-3}$) | $0.956 \pm 0.002$ | $1.337 \pm 0.002$ |
| Micro-morphology | Semi-crystalline | Amorphous |
| Initial rod diameter | $20 \pm 0.1$ mm | — |
| Thickness | — | $155 \pm 5$ μm |
| Commercial | DFDY 6130 natural 77 | AK 30 |
| Supplier | Plastifab Inc., Montréal, Canada | Rhône-Poulenc Films Division, Lyon, France |

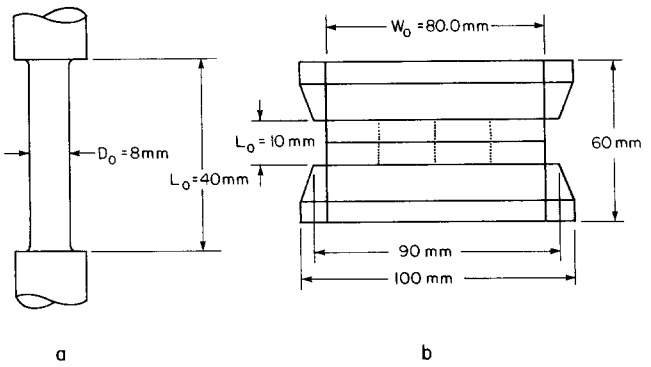


**Figure 1** Tensile specimens: (a) axisymmetric specimen; (b) film specimen

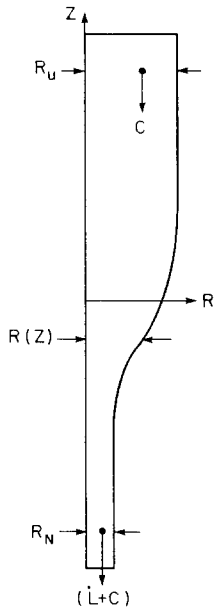


**Figure 2** Cylindrical polar coordinate system situated in the transition front and translating with it

connected by a lead to the chart recorder of the tensile machine. In this way, each photograph was associated with a precise overall elongation measured in the loaded condition.

*Temperature measurements*

Two methods were used to measure the temperature of the specimens. In the first method, applied to the axisymmetric specimens, a fine chromel–alumel thermocouple was put against the transition front and allowed to follow its propagation.

The second method uses the infrared technique to obtain the temperature distribution of a film specimen. To perform this, an infrared camera A.G.A. 680 was utilized. The calibration details of this technique are reported in Reference 11.

## CHARACTERIZATION PROCEDURE

The geometrical characterization was performed using a procedure given in Reference 4. This procedure originally developed for the axisymmetric specimens, was extended to plane-strain specimens in Reference 5.

For the axisymmetric specimens, a cylindrical polar coordinate system $(r, \theta, z)$, situated in the transition front, is assumed (*Figure 2*). The profile of the specimen is approximated using the following two-parameter description:

$$\bar{R}(\bar{z}) = \frac{1}{2}[(1 + \bar{R}_N) + (1 - \bar{R}_N)\tanh(\beta_A \bar{z})] \quad (1)$$

where a bar represents a normalization by the unnecked section radius $R_U$, $\beta_A$ is a measure of the sharpness of the transition front, $\bar{R}_N$ designates the normalized radius of the necked section, and $\bar{z}$ refers to the coordinate along the specimen axis.

The effective strain in the unnecked section $\varepsilon_U$ was calculated using the expression

$$\varepsilon_U = 2\ln(R_0/R_U) \quad (2)$$

where $R_0$ is the initial radius.

Similarly, using a Cartesian coordinate system $(x, y, z)$, the profile of a film specimen is approximated by

$$\bar{h}(\bar{z}) = \frac{1}{2}[1 + \bar{h}_N + (1 - \bar{h}_N)\tanh(\beta_f \bar{z})] \quad (3)$$

where a bar represents a normalization by the half-thickness of the unnecked section, $h_U$, $\beta_f$ is a measure of the sharpness of the transition front in a film specimen, and $\bar{h}_N$ is the normalized semi-thickness of the necked section.

Here the effective strain in the unnecked section $\varepsilon_U$ was computed using the expression

$$\varepsilon_U = \frac{3^{1/2}}{2}\ln(h_0/h_U) \quad (4)$$

where $h_0$ is the initial half-thickness.

In addition to the geometrical characterization, the maximum nominal stress $N_{max}$ (corresponding to neck initiation) and the propagation nominal stress $N_P$ were obtained from the overall load–stretch curve using the following expressions:

$$N_{max} = \frac{P_{max}}{A_0}, \qquad N_P = \frac{P_P}{A_0} \quad (5)$$

where $A_0$ is the initial section area and $P_{max}$ and $P_P$ are the maximum and propagation loads, respectively.

All the previous parameters corresponding to axisymmetric specimens were systematically displayed as functions of a non-dimensional velocity parameter $V_A$ defined as follows:

$$V_A = \dot{L}/(R_U S \dot{\varepsilon}_R) \quad (6)$$

where $\dot{L}$ is the elongation rate, $S$ represents the number of transition fronts existing in the specimen, and $\dot{\varepsilon}_R$ is a reference strain rate (equal to unity for the present work).

Similarly, all the parameters corresponding to the film specimens were systematically displayed as a function of a non-dimensional velocity parameter $V_F$ defined as follows:

$$V_F = \dot{L}/(h_U S \dot{\varepsilon}_R) \quad (7)$$

## RESULTS

### *Evolution of the specimens during stretching*

A typical set of axisymmetric specimen profiles, showing neck propagation, is presented in *Figure 3* for a test carried out at 26.4°C and $1 \times 10^{-2}$ mm s$^{-1}$. *Figure 3a* shows the specimen in its unloaded state. *Figure 3b* shows it at a stretch $\lambda = 1.12$ corresponding to the maximum load point. *Figures 3c–e* show the specimen at three different stretching ratios $\lambda$ equal to 1.75, 2.5, and 3.25. Note that the neck spreads almost uniformly after a stretch of $\lambda = 1.75$.

The overall load–stretch curve of this test is shown in *Figure 4*. As previously mentioned, this curve shows a load maximum, followed by a gradual unloading to about two-thirds of the maximum load. With further straining,

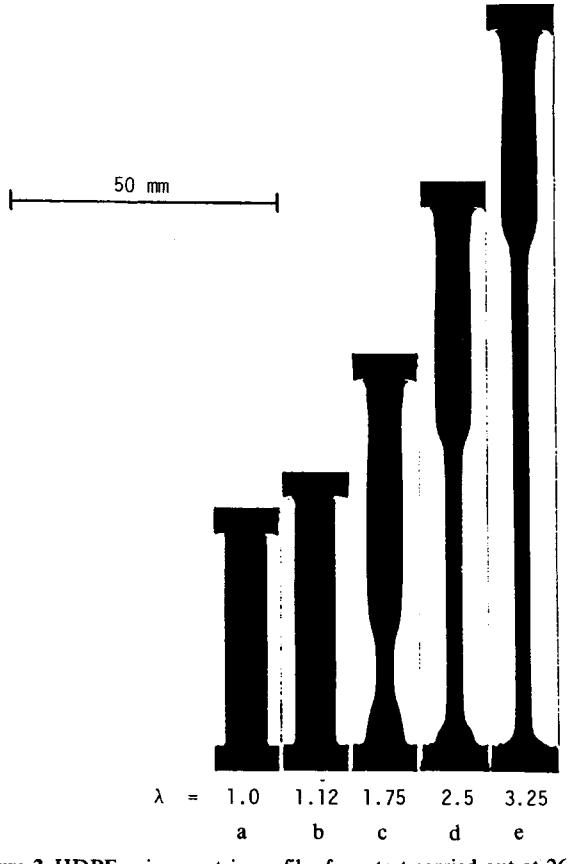


**Figure 3** HDPE axisymmetric profiles for a test carried out at 26.4°C and $1 \times 10^{-2}$ mm s$^{-1}$ at increasing stretch ratios $\lambda$

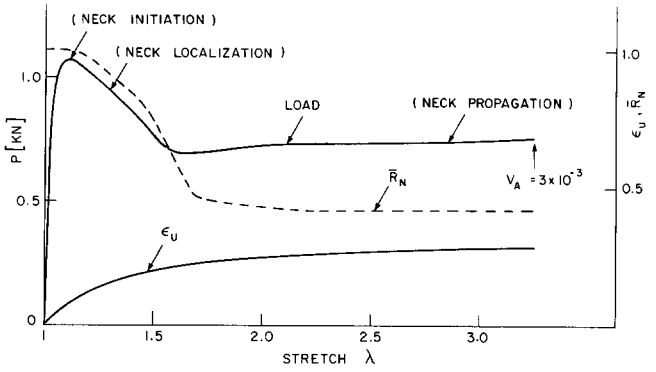


**Figure 4** Experimental load–stretch curve and evolution of the unnecked section strain $\varepsilon_U$ and necked section normalized radius $\bar{R}_N$ for the test in *Figure 3* on HDPE

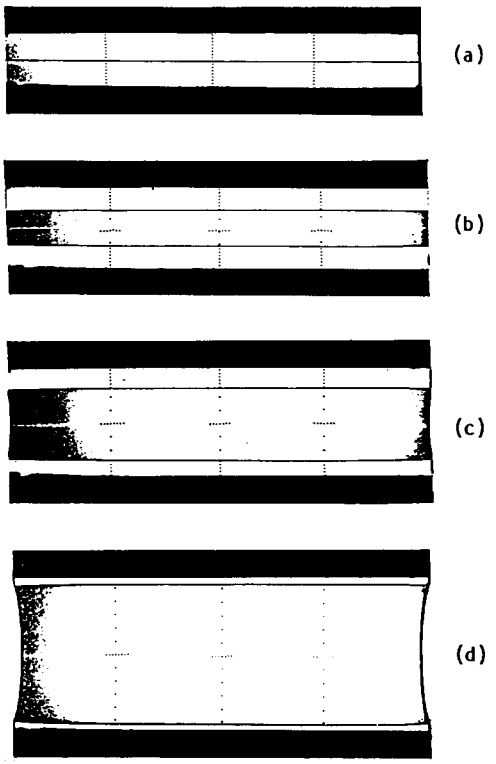


**Figure 5** Stretching of a PET film specimen at 20°C and 0.05 mm s$^{-1}$: (a) $\lambda = 1.0$; (b) $\lambda = 1.5$; (c) $\lambda = 2.0$; (d) $\lambda = 3.0$. $w_0 = 80.0$ mm; $l_0 = 10.0$ mm; $h_0 = 155 \pm 2$ $\mu$m

a small load increase takes place until a load plateau corresponding to neck propagation is reached.

In the same figure, the evolution of the normalized radius of the necked section $\bar{R}_N$, and the effective strain of the unnecked section $\varepsilon_U$ are displayed. We can observe that $\bar{R}_N$ diminishes gradually with the stretching ratio to a value of approximately 0.4, while $\varepsilon_U$ increases to a value of approximately 0.3.

For the PET film specimens, *Figure 5* shows four photographs of a plane-strain test performed at 20°C and 0.05 mm s$^{-1}$. *Figure 5a* shows the specimen mounted in the jaws of the tension machine before the start of the test. The white central region is the calibrated zone. The jaws are visible in black above and below. The horizontal central line is the initial defect. *Figures 5b–d* show the specimen at three different stretching ratios $\lambda$ equal to 1.5, 2.0 and 3.0, respectively. A central band appears at

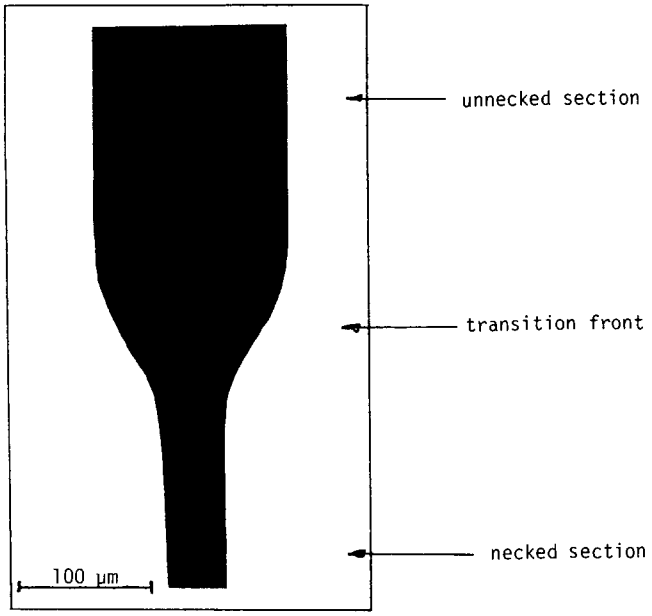


**Figure 6** Transverse section of the upper transition front of the film specimen shown in *Figure 5*

the initial defect and spreads along the specimen, while straining proceeds. In this zone, the markers are separated by a distance several times that in the rest of the specimen. Both the vertical and horizontal marker rows remain straight and always separated by the same distance, thus indicating that plane-strain conditions hold in the specimen while it is stretched. The two horizontal lines separating this region from the rest of the specimen are the transition fronts.

At a finer scale, *Figure 6* shows a microphotograph of the upper transition front of the specimen of *Figure 5*. The profile geometries of these fronts are very similar to those of the axisymmetric specimens. Also, the length of the transition front is almost equal to the thickness of the unnecked section.

The overall load–stretch curve corresponding to the plane-strain test is displayed in *Figure 7*. This curve shows an initial quasilinear portion followed by a very short yield transition and then a large plateau corresponding to plane-strain neck propagation. It is interesting to note that the load maximum at yield that appears in the axisymmetric test does not exist in the present case, probably because of the magnitude of the initially introduced defect. In the same figure, the evolution of the normalized half-thickness $\bar{h}_N$ of the necked section and the effective strain of the unnecked section $\varepsilon_U$ are shown. The two parameters reach a plateau after a stretch $\lambda = 1.2$.

*HDPE – axisymmetric neck propagation*

For the axisymmetric profile the evolution of the geometry after a stretch $\lambda = 3.0$ virtually ceases (*Figure 4*). As a result, we have chosen this stretch as our standard value to report the global results. The following information is related to the physical state of the specimens at $\lambda = 3.0$ (except for the maximum load stress $N_{max}$ of *Figure 13*). The temperature rise at the surface of the axisymmetric specimens (in the transition front), due to plastic deformation, is displayed as a function of the non-dimensional velocity parameter $V_A$ in *Figure 8*. Since the temperature gradient between the centre and the surface of the specimens is relatively small, this temperature rise can be taken as a good approximation of the volume average temperature increase. In *Figure 8*, for $V_A < 3 \times 10^{-3}$, neck propagation can be considered as isothermal (dashed line), while for larger values neck propagation occurs under non-isothermal conditions (solid lines). The evolution of the normalized necked section radius $\bar{R}_N$ and of the effective strain at the unnecked section $\varepsilon_U$ of the axisymmetric specimens is displayed, as a function of the previous velocity parameter, in *Figures 9* and *10*, respectively. Under isothermal

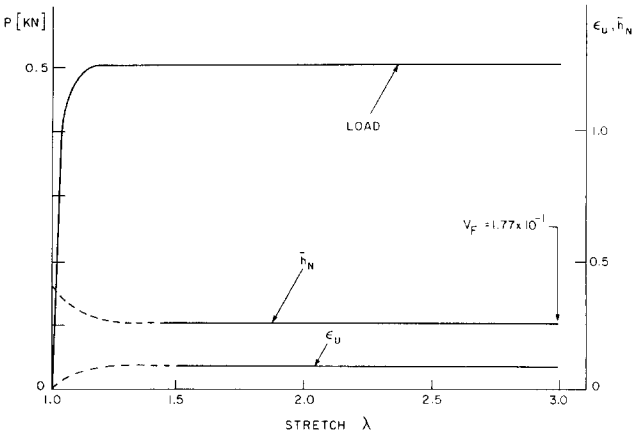


**Figure 7** Experimental load–stretch curve and evolution of the unnecked section strain $\varepsilon_U$ and necked section half-thickness $\bar{h}_N$ for a PET film at 20°C and $5.0 \times 10^{-2}$ mm s$^{-1}$

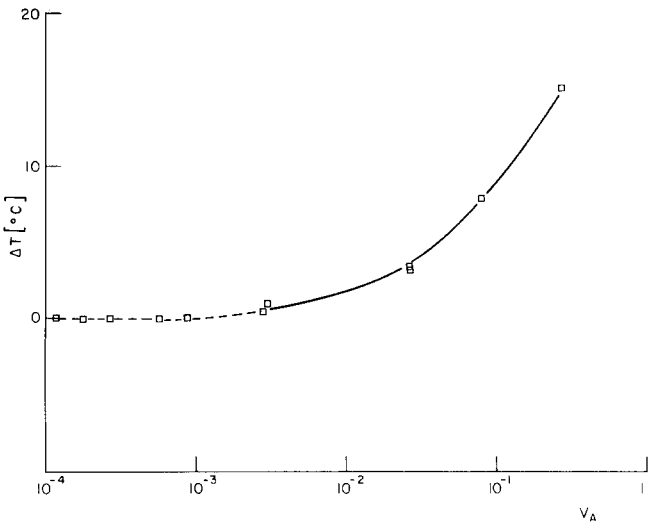


**Figure 8** Temperature rise due to plastic deformation in the HDPE axisymmetric specimens; $\lambda = 3.0$; $T_0 = 25$°C

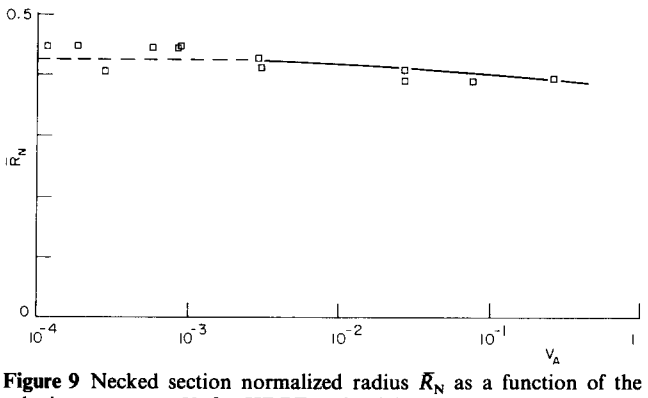


**Figure 9** Necked section normalized radius $\bar{R}_N$ as a function of the velocity parameter $V_A$ for HDPE at $\lambda = 3.0$

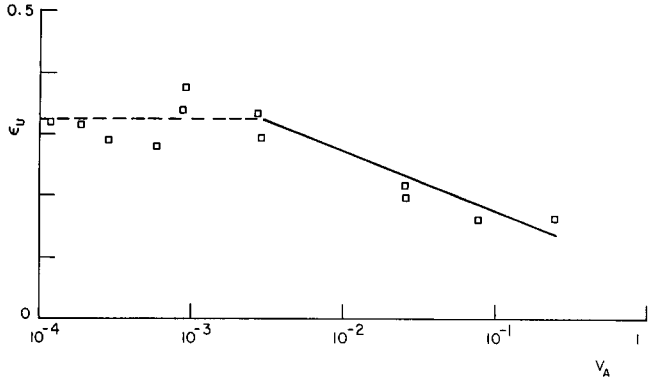


**Figure 10** Effective strain of unnecked section $\varepsilon_U$ as a function of the velocity parameter $V_A$ for HDPE at $\lambda = 3.0$

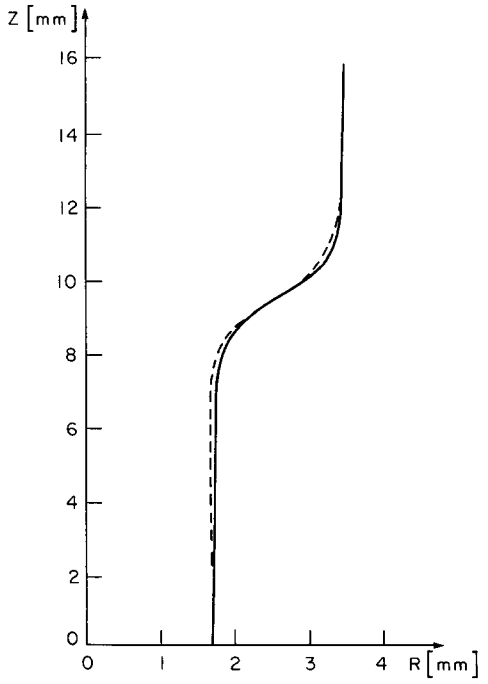


**Figure 11** Comparison between an experimental profile (——) and the corresponding analytical profile (– – –) obtained by fitting the expression (1) for HDPE at 25°C and $1.0 \times 10^{-2}$ mm $s^{-1}$

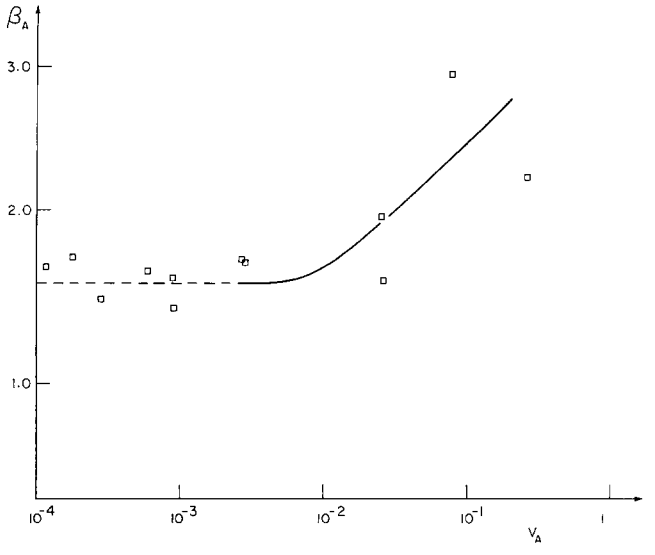


**Figure 12** Parameter $\beta_A$ as a function of the velocity parameter $V_A$ for HDPE at $\lambda = 3.0$

conditions, $\bar{R}_N$ and $\varepsilon_U$ are practically independent of velocity. On the other hand, under non-isothermal conditions, $\bar{R}_N$ and $\varepsilon_U$ decrease when the velocity parameter $V_A$ increases.

In *Figure 11*, we compare the experimental neck profile (solid line) of the specimen shown in *Figure 3* with the corresponding analytical profile (dashed line) obtained by fitting equation (1). A satisfactory correlation between the experimental and analytical profiles is observed, even though the analytical profile tends to underestimate the convex and overestimate the concave curvatures of the experimental transition front.

*Figure 12* shows the evolution of the parameter $\beta_A$ with the velocity parameter. We note that this parameter is almost independent of the velocity under isothermal conditions, while it increases under non-isothermal conditions.

*Figure 13* shows the evolution of the maximum nominal stress $N_{max}$ and the propagation nominal stress $N_P$ as a function of the velocity parameter $V_A$. Both stresses increase with increasing $V_A$. However, the increase of $N_{max}$ is greater than that of the $N_P$. Also, in both cases, the increase is greater under isothermal conditions than under non-isothermal conditions.

*PET – plane-strain neck propagation*

*Figures 14–18* show the corresponding plane-strain test

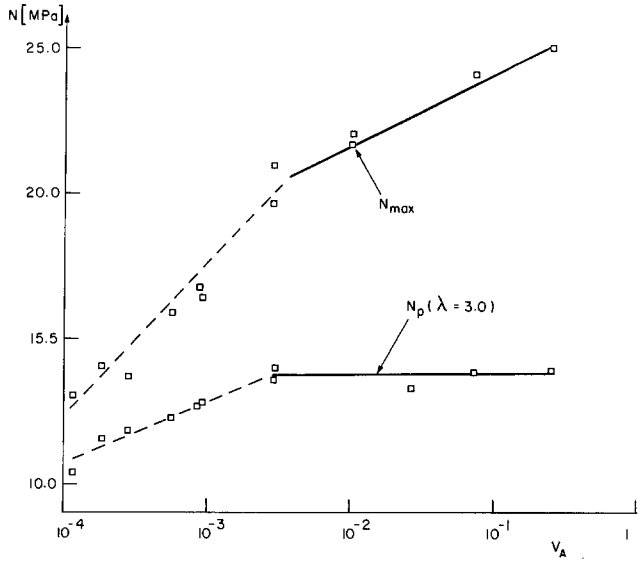


**Figure 13** Maximum nominal stress ($N_{max}$) and propagation nominal stress ($N_P$) as functions of the velocity parameter $V_A$ for HDPE

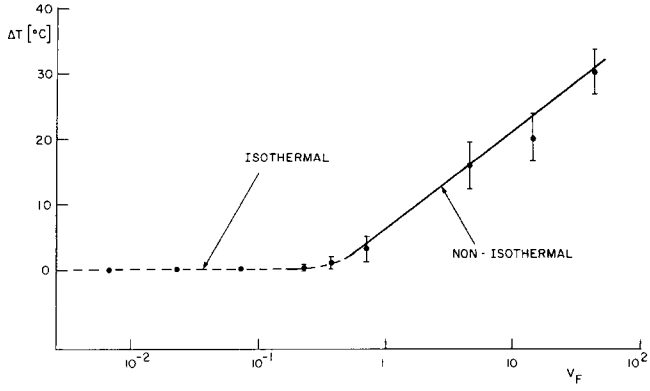


**Figure 14** Temperature rise ($\Delta T$) due to plastic deformation in the PET film specimens

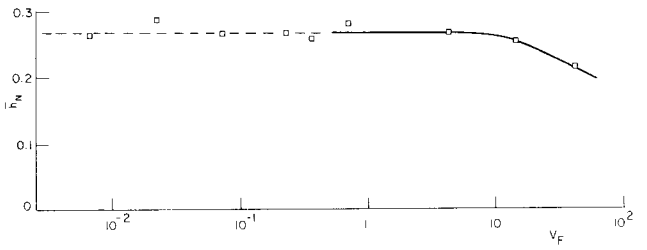

**Figure 15** Necked section half-thickness $\bar{h}_N$ as a function of the velocity parameter $V_F$ for PET film at $\lambda = 3.0$

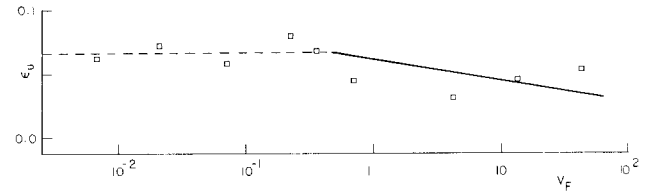

**Figure 16** Effective strain of unnecked section $\varepsilon_U$ as a function of the velocity parameter $V_F$ for PET film at $\lambda = 3.0$

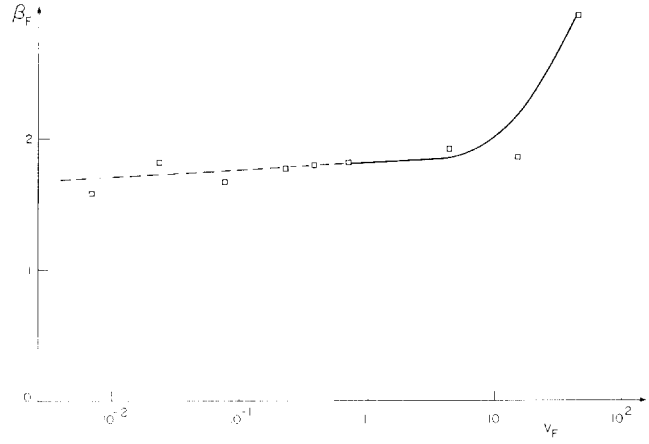

**Figure 17** Parameter $\beta_F$ as a function of the velocity parameter $V_F$ for PET film at $\lambda = 3.0$

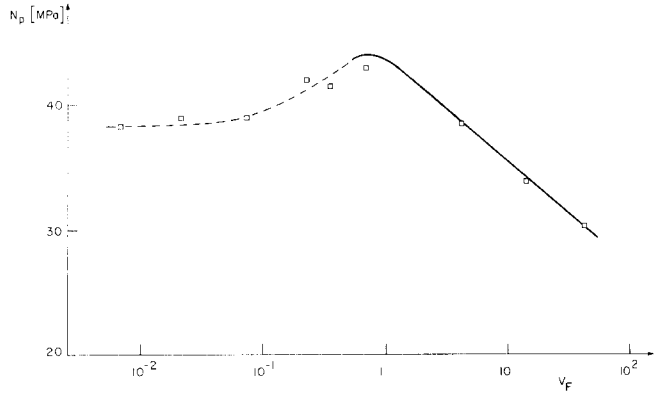

**Figure 18** Propagation nominal stress $N_P$ as a function of the velocity parameter $V_F$ for PET film at $\lambda = 3.0$

results as a function of the non-dimensional plane-strain velocity parameter $V_F$.

In *Figure 14*, the temperature rise is displayed as a function of the velocity parameter. Isothermal conditions prevail up to a velocity $V_F \simeq 0.5$ ($\dot{L} = 7.5 \times 10^{-2}$ mm s$^{-1}$). Thereafter, the temperature increases steadily with increasing velocity. This result is in good agreement with the temperature calculations reported in Reference 8.

In *Figures 15–17*, we observe the same general tendencies as for the HDPE axisymmetric specimens. Therefore, we can conclude that these tendencies are general in character, independent of the type of thermoplastic polymer used and of the type of tensile test performed.

In *Figure 18*, note that, contrary to the HDPE case, the propagation nominal stress $N_P$ diminishes with increasing velocity $V_F$, under non-isothermal conditions. This is simply because PET has higher thermal sensitivity than HDPE[11,18]. A very similar result was reported in Reference 3.

## DISCUSSION

The stress–strain relations for HDPE and PET were reported in References 11 and 13. In these studies the experimental relations were fitted using a multiplicative model of the following type:

$$\sigma = \kappa f(\varepsilon)(\dot{\varepsilon}/\dot{\varepsilon}_R)^m \tag{8}$$

where $\sigma$, $\varepsilon$ and $\dot{\varepsilon}$ are the effective stress, strain and strain rate, respectively, $\kappa$ is a scale factor, and $m \equiv [\partial(\ln \sigma)/\partial(\ln \dot{\varepsilon})]_\varepsilon$ is the strain rate sensitivity. In *Table 2* specific values of the parameters of equation (8) are given for both materials. Using the above model, the strain hardening coefficient $\gamma \equiv [\partial(\ln \sigma)/\partial(\ln \varepsilon)]_{\dot{\varepsilon}}$ is given by the following expression:

$$\gamma = \frac{\partial \ln f(\varepsilon)}{\partial \varepsilon} \tag{9}$$

According to rate-independent instability theory[7,14,15], a neck can develop in a perfect specimen when $\gamma$ passes from a value $>1$ to a value $<1$. This occurs at the load maximum[16]. Using the data of *Table 2* for HDPE, we find that this should take place at an effective strain $\varepsilon = 0.12$. In *Figure 4*, we notice that a neck is formed ($\bar{R}_N < 1$) at an effective strain of $\varepsilon \sim 0.113$ ($\lambda \sim 0.12$) in the HDPE axisymmetric specimens. We can thus conclude that a satisfactory correlation between the theory and the experiment is observed here. However, we observe, in the same figure, that the unnecked section continues to deform in a stable way beyond this instability value up to a value as high as $\varepsilon_U = 0.29$. This leads us to ask why a series of multiple necks does not form in the unnecked section.

**Table 2** Values of parameters in equation (8) for HDPE and PET

| | Temperature range (°C) | Strain rate range (s$^{-1}$) | $\kappa$ (MPa) | $w^a$ | $H^a$ | $\dot{\varepsilon}_R$ (s$^{-1}$) | $m$ |
|---|---|---|---|---|---|---|---|
| HDPE | $25 \pm 2$ | $1 \times 10^{-3}$–$1 \times 10^{-5}$ | $43.0 \pm 1^b$ | $28.5 \pm 1^b$ | $0.33 \pm 0.03^b$ | $1.0^b$ | $0.075 \pm 0.01^b$ |
| PET | $20 \pm 1$ | $3 \times 10^{-3}$–$1 \times 10^{-4}$ | $51.0 \pm 1^c$ | $65 \pm 5^c$ | $0.53 \pm 0.03^c$ | $1.0^c$ | $0.03 \pm 0.002^c$ |

[a] $w$ and $H$ are parameters in the expression for $f(\varepsilon)$: $f(\varepsilon) = [1 - \exp(-w\varepsilon)] \exp(H\varepsilon^2)$
[b] After References 13 and 18
[c] After References 11 and 12

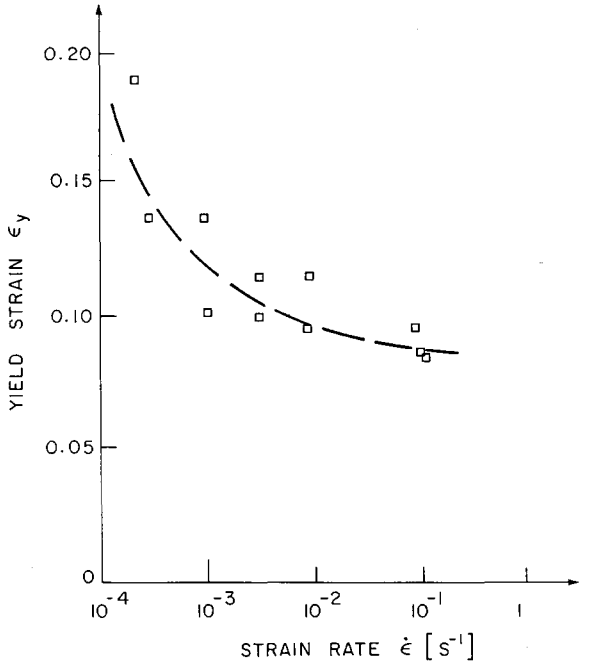


**Figure 19** Yield strain $\varepsilon_y$ as a function of the strain rate $\dot{\varepsilon}$ (after Reference 13) for HDPE hour-glass specimens at 25°C

To attempt to answer this question, we note that the only major difference between the physical state of a material portion in the unnecked section before and after the neck localization is the effective strain rate, which diminishes from a value close to the nominal strain rate $\dot{\varepsilon}_N$ (elongation rate/initial length) to a value several times smaller. It has been demonstrated[3,17] that, at small strain rates, amorphous polymers show a more important viscoelastic behaviour than at high strain rates. This behaviour is controlled by the molecular diffusion and does not favour strain localization to the same extent as the elastic–plastic response present at high strain rates[3].

Another important factor is the shift toward high values of yield strain $\varepsilon_y$ (maximum load strain) when the strain rate diminishes. *Figure 19* shows this effect in HDPE hour-glass specimens stretched at constant strain rates[13]. At high strain rates the yield strain is $\approx 0.09$, while at small ones it increases to $\approx 0.15$. It is evident that the instability point also shifts in the same direction, thus permitting a stable deformation at higher strains, when the strain rate diminishes. It is likely that the combined effects of these result in the stable deformation of the unnecked region of the HDPE.

Similarly for the PET, $\gamma$ passes from a value $>1$ to a value $<1$ at an effective strain $\varepsilon = 0.06$. Since, for the test of *Figure 7*, $\varepsilon_U$ is $\approx 0.09$, it is evident that the above question also arises.

## CONCLUSIONS

Three principal conclusions can be drawn from this study:

(1) Neck propagation occurs under isothermal conditions, for HDPE axisymmetric specimens for values of the velocity parameter $< 3 \times 10^{-3}$, and for PET films for values $< 5 \times 10^{-1}$.

(2) The geometry of the travelling neck is almost independent of the velocity parameter under isothermal conditions, while an important evolution of the geometry is observed under non-isothermal conditions. The general trends of this evolution are probably independent of the type of thermoplastic polymer considered and the type of tensile test performed.

(3) An unexpected stability of the plastic deformation is observed in the unnecked section of the specimens of both materials. It is probable that this stability has been produced by the combined effects of a change in the molecular mechanisms of deformation (from the plastic to the viscoelastic behaviour), and an increase of the yield strain value, when the strain rate decreases.

## ACKNOWLEDGEMENTS

This work was supported in part by the Natural Sciences and Engineering Research Council of Canada (Grants A-4479, G-1679) and the Government of the Province of Québec (Programme FCAR). A.M.-L. is grateful to the Mexican Council for Science and Technology (CONACYT) for the award of a Graduate Fellowship (1982–1986) during which this work was initiated.

## REFERENCES

1 G'Sell, C., Marquez-Lucero, A., Souahi, A. and Tong, Y. S. in 'Proceedings of an International Symposium on Plastic Instability, Paris', Les Presses de l'Ecole Nationale des Ponts et Chaussées, Paris, 1985, p. 159
2 Engelaere, J. C., Cavrot, J. P. and Rietsch, F. *Eur. Polym. J.* 1979, **16**, 721
3 Ward, I. M. in 'Mechanical Properties of Solid Polymers', Wiley-Interscience, London, 1971
4 Hutchinson, J. W. and Neale, K. W. *J. Mech. Phys. Solids* 1983, **31**, 405
5 Tugcu, P. and Neale, K. W. *Int. J. Solids Struct.* 1987, **23**, 1063
6 G'Sell, C., Aly-Helal, A. and Jonas, J. J. *J. Mater. Sci.* 1983, **18**, 1731
7 Vincent, P. I. *Polymer* 1960, **1**, 7
8 Hookway, D. C., *J. Text. Instr.* 1958, **49**, 292
9 Stokes, V. K. and Nied, H. F. *J. Eng. Mater. Technol.* 1986, **108**, 107
10 G'Sell, C. and Jonas, J. J. *J. Mater. Sci.* 1979, **14**, 583
11 Marquez-Lucero, A. *Doct.-Ing. Thesis* INPL, Nancy, France, 1986
12 Marquez-Lucero, A. and G'Sell, C., unpublished
13 G'Sell, C. and Souahi, A., unpublished
14 Nadai, A. in 'Theory of Flow and Fracture of Solids', McGraw-Hill, New York, 1950
15 Haward, R. N. in 'The Physics of Glassy Polymers', Applied Science, London, 1973
16 G'Sell, C., Marquez-Lucero, A., Gilormini, P. and Jonas, J. J. *Acta Metall.* 1985, **33**, 759
17 Ward, I. M. *J. Mater. Sci.* 1971, **6**, 1397
18 Aly-Helal, N. A. *Doct.-Ing. Thesis* INPL, Nancy, France, 1982